Geological Quarterly, 2024, 68: 24
DOI: http://dx.doi.org/10.7306/gq.1752

# Trace elements and garnet formation in a distal skarn zone: a case study of the Rudnik deposit, Central Serbia

Bojan KOSTIĆ[1, *], Pavle TANČIĆ[2] and Natalija BATOĆANIN[3]

[1] University of Belgrade, Faculty of Mining and Geology, Djušina 7, 11000 Belgrade, Serbia; ORCID: 0000-0002-9879-5547

[2] University of Belgrade, Institute of Chemistry, Technology and Metallurgy, Department for Catalysis and Chemical Engineering, Njegoševa 12, 11000 Belgrade, Serbia; ORCID: 0000-0002-4024-710X

[3] University of Belgrade, Faculty of Geography, Studentski trg 3, 11000 Belgrade, Serbia; ORCID: 0000-0002-9879-5547

Kostić, B., Tančić, P., Batoćanin, N., 2024. Trace elements and garnet formation in a distal skarn zone: a case study of the Rudnik deposit, Central Serbia. Geological Quarterly, 2024, 68, 24; https://doi.org/10.7306/gq.1752

The Rudnik Pb-Zn deposit is hosted in skarns and hornfels formed in the late Oligocene by contact metamorphism of limestones, sandstones and shales. Garnets, together with epidote, represent the main non-metallic minerals in the Rudnik skarn. In the distal skarn zone, the garnets are rare and their occurrence is related to the flow path of hydrothermal fluids. To constrain the hydrothermal and physicochemical conditions, *in situ* elemental SEM-WDS and LA-ICP-MS analyses, and fluid inclusion microthermometric measurements, were made. The Rudnik garnets from the distal skarn zone are predominantly of andradite-grossular composition ($Adr_{39.3–88.9}Grs_{2.9–53.9}Alm_{0.5–10.0}$), with a small amount of spessartine. Generally, the Fe-rich garnets show a positive Eu anomaly with LREE enrichment and a HREE flat pattern, with homogenization temperatures and salinities of fluid inclusions ranging from 373 to 392°C and from 14.25 to 15.27% NaCl equivalent, respectively. The trace elements and microthermometric properties indicate that the garnets formed at moderately high temperatures, mildly acidic pH levels and increased oxygen fugacity.

Key words: garnet geochemistry, REE, fluid inclusion, conditions, Rudnik skarn deposit.

## INTRODUCTION

Garnets are common in metamorphic and skarn deposits, and can be a helpful tool in prospecting (Yardley et al., 1991). Despite their highly variable composition reflecting a number of elemental substitutions in the crystal structure, the composition of garnet can reflect the alteration history during water/rock (W/R) interchange reactions (Somarin, 2004). One of the main characteristics of garnet is fractionation of rare earth elements (REEs) (Gaspar et al., 2008). The application of REEs to study the effects of hydrothermal fluids in skarn systems, and modern methods such as LA-ICPMS analyses, have been recently introduced to better understand the trace element chemistry of garnet. As REEs have commonly been regarded as insensitive to all except hydrothermal processes, grossular and andradite (grandite) solid-solution garnets have been widely used to infer the hydrothermal fluid evolution of skarn deposits, in which they are common (Somarin, 2004 and references therein); many studies of REEs in garnets have been made (e.g., Jamtveit and Hervig, 1994; Nicolescu et al., 1998; Smith et al., 2004; Gaspar et al., 2008; Zhai et al., 2014; Park et al., 2017; Xiao et al., 2018; Kostić et al., 2021).

Changes in hydrothermal systems can result in chemical zonation patterns during garnet growth, as widely discussed (e.g., Jamtveit et al., 1993, 1995; Pollok et al., 2001; Tančić et al., 2012; Kostić et al., 2021). Oscillatory zoning in skarn minerals, particularly in grandite garnets, is common in shallow contact metamorphic aureoles (Smith et al., 2004).

In Serbia, three locations with optically anisotropic and oscillatory zoned grandite garnets in skarns have been characterized: Tančić et al. (2012, 2020) at Kopaonik Mt.; Srećković-Batoćanin et al. (2014) at Rogozna Mt.; and Kostić et al. (2021) at Rudnik Mt.

This study describes the Rudnik garnets obtained from borehole samples, and determined by in situ analyses of major and trace elements, using SEM-WDS, LA-ICP-MS, and microthermometric measurements of garnet fluid inclusions in order to investigate their geochemical characteristics and reveal the physicochemical conditions of the hydrothermal fluids. As previously shown (Kostić et al., 2021), the REE trends observed also help understand the mechanisms by which trace elements and REEs become incorporated into garnets.

* Corresponding author, e-mail: bojan.kostic@rgf.bg.ac.rs
Received: October 21, 2023; accepted June 3, 2024; first published online: September 2, 2024

## GEOLOGICAL SETTING

The Rudnik skarn deposit is located on the central axis of the Sava Zone, interpreted as a suture zone of the northern section of the Neotethys Ocean (Schmid et al., 2008). Generally, the geology of the central Balkan Peninsula reflects the whole evolution of the Vardar Ocean, as a part of the Neotethys. This evolution includes Permian-Triassic opening, Late Jurassic ophiolite obduction, Cretaceous subduction and Cenozoic post-collisional orogenic development (see Schmid et al., 2008; Cvetković et al., 2016; Prelević et al., 2017). The Sava Suture Zone separates the Carpatho-Balkan orogen from southerly and westerly Adria derived thrust sheets of the Dinarides (Pamić and Šparica, 1983; Haas and Péró, 2004). Trending NNE from Belgrade, the Sava Zone is mostly represented by Upper Cretaceous flysch.

In the vicinity of Rudnik Mt., the Cretaceous flysch deposits (Fig. 1) have been described as clastic „paraflysch“ (Anđelković, 1973; Dimitrijević and Dimitrijević, 2009), i.e., a typical flysch, but lacking the characteristic internal organization. Lower Cretaceous strata are represented by sandstones, siltstones and limestones, which commonly look like immature turbidites (Dimitrijević and Dimitrijević, 1987, 2009; Sladić-Trifunović et al., 1989). The Upper Cretaceous succession is represented by Albian-Cenomanian conglomerates, microconglomerates, sandstones, carbonates and continental shales (Brković, 1980). These Cretaceous carbonate-sandstone-shale sequences are cut by numerous quartz-latitic stocks and dykes dated to the Oligocene-Miocene boundary at 23 Ma (Cvetković et al., 2016; Kostić et al., 2021). There is no evidence of any plutonic intrusive body as a source of these dykes. Contact metamorphic aureoles were formed at some places along the contact between the quartz-latite dykes and Cretaceous clastic flysch deposits. In the contact zone, metasedimentary rocks, hornfels and skarns host polymetallic Pb-Zn mineralization which typically consists of pyrrhotite, galenite, sphalerite, chalcopyrite and arsenopyrite with small amounts of magnetite, cassiterite and scheelite. The ore bodies are highly variable in size and shape (Stojanović et al., 2018). Lateral zoning is weakly dispayed in the contact aureole of the southern part of Rudnik skarn deposit, and the skarn mineralogy shows close correlation with that of the protolith. Petrographic observations indicate that the most common minerals in the skarns are quartz, epidote, zoisite, chlorite, calcite, and also the minerals of the actinolite-tremolite group. More skarnized zones include garnets and pyroxenes. Miocene strata (conglomerates and sandstones) cover only a small area to the NW and SE of Rudnik, with a small metamorphic aureole which can be observed along the contact zone with quartzlatitic dykes.

## ANALYTICAL METHODS

*In situ* major element analysis was carried out using a *JEOL 6610 LV* scanning electron microscope equipped with a wavelength-dispersive spectrometer (Oxford Instruments Wave 700) at the Faculty of Mining and Geology, University of Belgrade. Analytical parameters were as follows: spot size 2 μm, an accelerating voltage of 30 kV and a probe current of 1.0 x $10^{-8}$ A, with 0.01% detection limit. Natural and synthetic mineral standards were used including albite (Al, Si), wollastonite (Ca), titanium monoxide (Ti), chromium oxide (Cr), and manganese (Mn) and iron (Fe) metals. Back-scattered (BSE) observations were conducted to reveal zoning and possible inclusions of other mineral phases within the garnet. Analyses were performed according to the observed zoning and avoiding the effects of inclusions.

Trace element analysis on garnets was performed by SEM-WDS using a *LA-ICP-MS* at the Geological Institute in Sofia (Bulgaria), using a *New Wave UP193FX LA* coupled to a *Perkin Elmer ICP-MS*. Laser ablation was executed using an ablation repetition rate of 8 Hz, with laser power of 8.5 J/cm$^2$; the size of ablation crater was 50 μm in diameter. The full ablation time was 90 s, which consisted of 20 s for pre-ablation, 50 s for ablation, and 20 s for the post-ablation signal. As external standard for fractionation correction, *NIST610* glass was analysed after every 10 analyses to correct systematic error. Data reduction was processed through Iolite software v2.5 (Paton et al., 2011), applying down-hole fractionation correction to all the analyses. The laser ablation produced a list of trace elements and rare earth elements (REEs).

Preparing garnet samples for microthermometric measurements of fluid inclusions involved a double-polished 130 micron-thin sample. Microthermometric data were obtained on a *LINKAM THMSG600* heating-freezing stage with a temperature range from –196 to +600°C, mounted on an *OLIMPUS BX51* microscope in the Fluid Inclusion Laboratory at the Faculty of Mining and Geology, University of Belgrade. Data reduction of microthermometric measurements was done with equations provided by Bodnar (1993). Measured inclusions are oriented in the direction of crystal growth and interpreted as primary in origin.

## RESULTS

### PETROGRAPHY

Garnet skarns are widely distributed in the Rudnik contact-metamorphic aureole near the contact with igneous rocks. The atypical occurrence of Rudnik skarns is reflected by the fact that there is no traceable mineralogical zonation at the surface. Clearer zonation can be observed in the borehole coordinates (44.120084°N, 20.520747°E). The sample 145 analysed was collected from a borehole at a depth of 195 m from the surface, the total length of the borehole being 559.8 m and ending in peridotite. The Cretaceous units penetrated by the borehole start from the top with coarse-grained conglomerate containing fragments/clasts of altered peridotite, chert and quartzite. These rocks are locally followed by alternating microconglomerates and sandstones. Below, sandstones continue on limestones with a greater or lesser terrigenous component through the borehole. Within the carbonate unit, depending on the siliciclastic content, marlstones, almost pure limestones and transitional varieties were recognized (Kostić et al., 2021). These carbonate rocks alternate with fine-grained rocks considered as hornfels that are composed of quartz, plagioclase, epidote, chlorite and diopside; depending on the contact distance certain minerals are absent from some parts of the rock. Conglomerate, sandstone and limestone display contact metamorphic alteration from metasedimentary rocks to skarns, where the skarns are more mineralogically interesting. Garnet-bearing skarns occur as small-scale bodies up to a few metres thick. Their texture is granoblastic and the structure is massive, rarely banded. The skarn samples selected for detailed analyses contain calcite + garnet + epidote

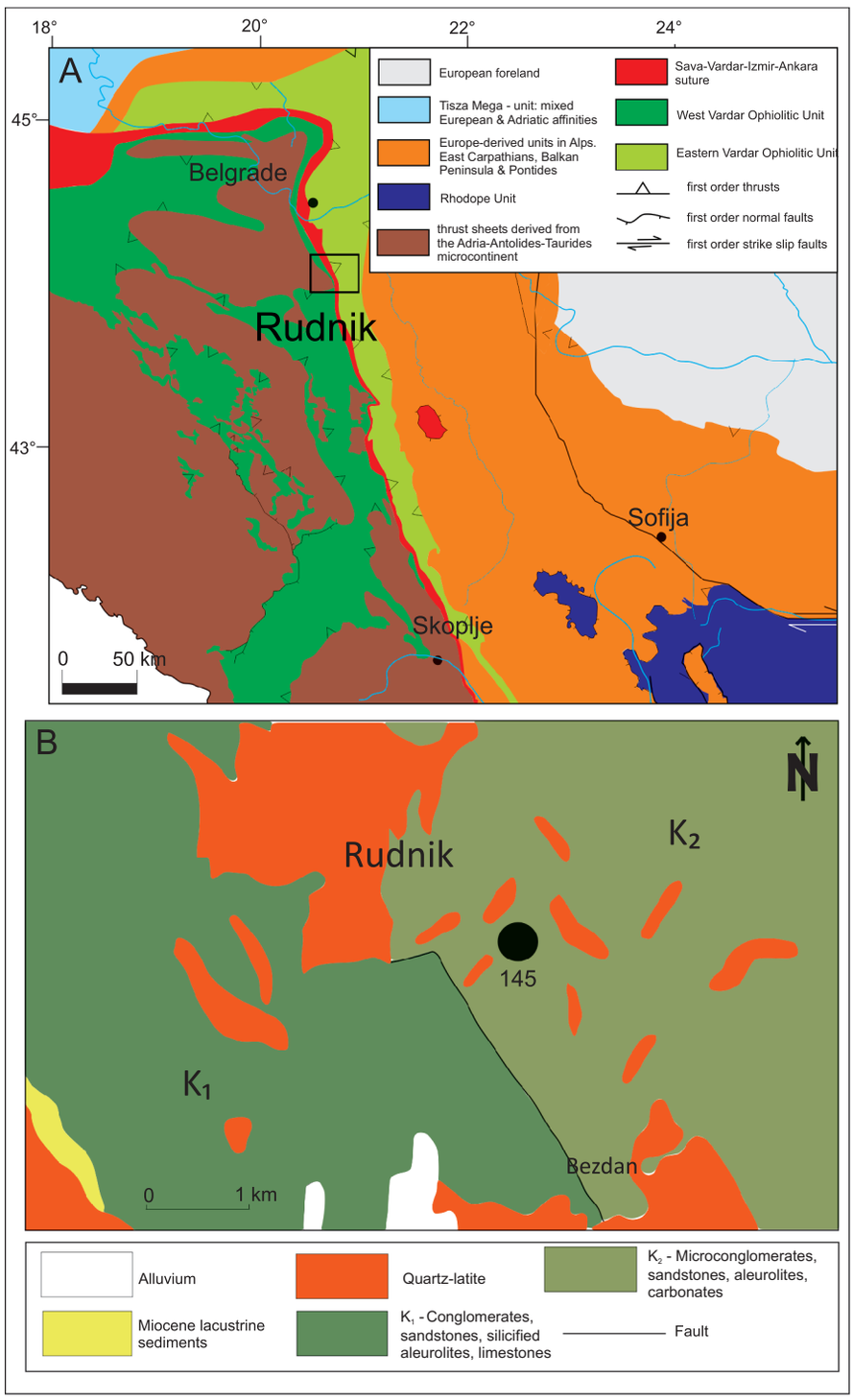


**Fig. 1A – simplified geological map of South-Eastern Europe (after Schmid et al., 2008), with the location of the study area within Serbia; B – simplified geological map of the Rudnik area modified according to the Basic Geological Map 1:100,000, Sheets Kragujevac (Brković et al., 1980) and Gornji Milanovac (Filipović et al., 1978)**

The location of sampling (no 145) is marked with a black dot

+ chlorite + quartz (Fig. 2). The garnet crystals show primarily anhedral granular texture under the microscope. The crystal size is mainly <1 mm, with rare small epidote inclusions. Common opaque minerals such as pyrrhotite, chalcopyrite and sphalerite (Stojanović et al., 2018) fill cavity spaces between euhedral anisotropic and oscillatory zoned garnet grains, which are rarely cross-cut by thin calcite veins. The SEM-WDS analyses show that an alternation of Al- and Fe-rich zones forms the oscillatory zoning. The epidote grains are anhedral and locally replaced by chlorite.

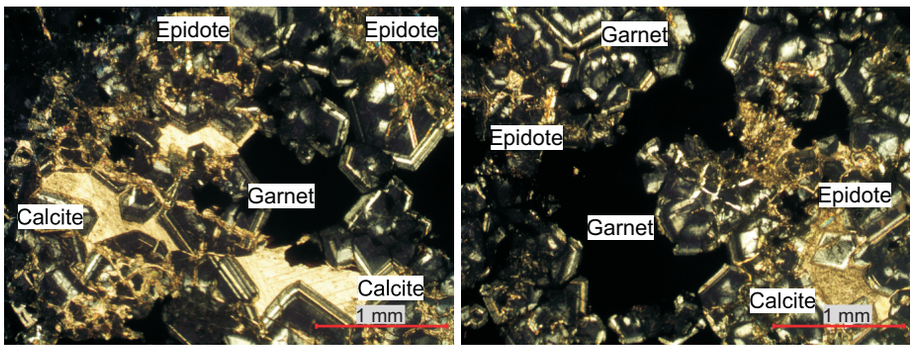


**Fig. 2. Photomicrograph showing anhedral granular texture of anisotropic oscillatory zoned garnets in skarn sample no. 145 taken from the borehole**

Characteristic occurrences of calcite and epidote are also presented, XPL; scale bar 1 mm

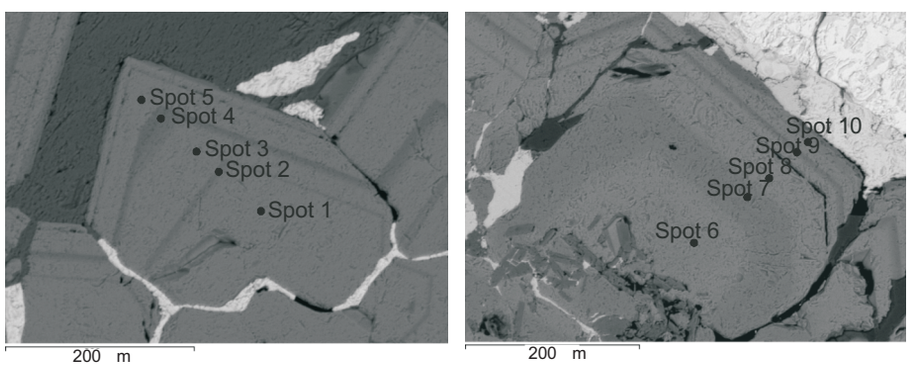


**Fig. 3. Back-scattered scanning electron microscope image of garnet grains with chlorite (left) and calcite (right)**

Black dots represent exact positions of the SEM-WDS and LA-ICP-MS analyses

## MAJOR ELEMENT GEOCHEMISTRY

The results from 10 representative SEM-WDS spot analyses on garnet grains (Fig. 3), indicate that the main components of the Rudnik garnets are $SiO_2$ (37.63–39.61 wt.%), $Al_2O_3$ (0–11.33 wt.%), CaO (33.04–35.03 wt.%) and FeO (13.72–27.26 wt.%). Compositionally, andradite and grossular predominate with minor almandine and spessartine components (Fig. 4). The FeO content obtained by SEM-WDS was converted to the ($FeO + Fe_2O_3$) sum, by assuming that the deficiency of total (Ti + Al + Cr) for the octahedral [Y] site is made up only of $Fe^{3+}$. Under BSE, garnets have visible compositional zoning where the zones with darker intensity are richer in Al, whereas lighter zones have a higher Fe content. The Mn content is <1 wt.%, while the Ti content is below the detection limit (Table 1). According to the results obtained, the garnets studied from the Rudnik orefield predominantly represent andradite-grossular solid solutions, being roughly of $Adr_{39.3–88.9}Grs_{2.9–53.9}Alm_{0.5–10.0}$ composition, and with minor amounts of spessartine (up to 1.8 mol%). SEM-WDS analyses indicate constant Ca contents in the core and the rim, albeit with small inclusions of epidote, quartz and rarely sphalerite in the grain cores.

## TRACE ELEMENT GEOCHEMISTRY

Data for the REEs and trace elements of the skarn garnets studied are shown in Table 2. In general, the Rudnik garnets are depleted in HREE elements and Sr relative to the primitive mantle (Table 2 and Fig. 5). In contrast, the U and Pb in the Rudnik garnets are enriched compared to the average primitive mantle (McDonough et al., 1995). Additionally, the pattern and

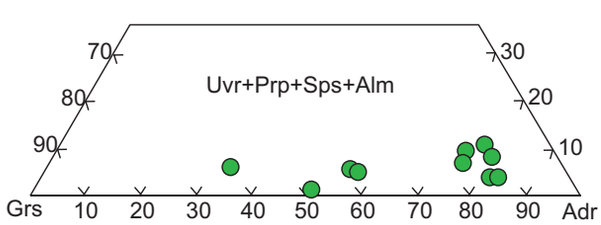


**Fig. 4. The ternary classification diagram for garnets (uvarovite, pyrope, spessartine and almandine in the octahedral [Y] sites)**

Grs – grossular, Adr – andradite, Uvr – uvarovite, Prp – pyrope, Sps – spessartine, Alm – almandine (based on Whitney et al., 2010)

obvious positive Eu anomaly is differs from previous results (Kostić et al., 2021) with no spatial relationship, as sample 145 is located in the hanging wall of the ore body. The trace element content of garnet in sample 145 is more variable then from garnets from the proximal zone of the mineralization by Kostić et al. (2021), and the garnets have more variable trace element contents, such as: Nb (0.009–0.249), Pb (0.013–2.32), Zr (0.153–3.82) and Hf (0.01–0.38).

## MICROTHERMOMETRIC RESULTS FROM THE FLUID INCLUSIONS

Observed and measured fluid inclusions in the Rudnik garnets occur as generally elongated and elliptical forms with less irregularly shaped inclusions. In general, the fluid inclusion populations are aqueous liquid-vapour inclusions (L-V) with maximum size of 5 μm. Representative heating and freezing data (Table 3 and Fig. 6) show the range of homogenization temper-

Table 1

**Representative SEM-WDS analyses of major elements in garnet sample 145 from the skarns studied (in wt.% oxides, rounded to the second decimal place), structural formula on the basis of 12 oxygen atoms per formula unit (apfu), and calculated end members (in mol%)**

| | Sample 145 | | | | | | | | | |
|---|---|---|---|---|---|---|---|---|---|---|
| | Spot 1 | Spot 2 | Spot 3 | Spot 4 | Spot 5 | Spot 6 | Spot 7 | Spot 8 | Spot 9 | Spot 10 |
| BSE | light | dark | light | dark | light | light | dark | light | dark | light |
| CaO | 33.28 | 34.31 | 33.04 | 34.46 | 33.35 | 33.91 | 34.79 | 33.5 | 35.03 | 33.64 |
| MnO | n.d. | n.d. | n.d. | 0.84 | 0.32 | 0.38 | 0.37 | n.d. | 0.47 | 0.36 |
| FeO | 27.06 | 19.99 | 26.91 | 13.72 | 25.97 | 25.68 | 19.77 | 27.26 | 16.13 | 26.21 |
| $Al_2O_3$ | n.d. | 7.36 | 0.66 | 11.33 | 1.58 | 1.98 | 6.64 | 0.37 | 10.11 | 1.35 |
| $SiO_2$ | 38.86 | 39.21 | 39.32 | 39.61 | 38.69 | 37.63 | 39.28 | 39.01 | 38.13 | 37.86 |
| Total | 99.20 | 100.87 | 99.93 | 99.96 | 99.91 | 99.58 | 100.85 | 100.14 | 99.87 | 99.42 |
| Garnet formula calculated on the basis of 12 oxygen atoms per formula unit (apfu) | | | | | | | | | | |
| Si | 3.200 | 3.095 | 3.210 | 3.105 | 3.150 | 3.069 | 3.104 | 3.180 | 3.006 | 3.100 |
| Al | 0.200 | 0.779 | 0.273 | 1.151 | 0.301 | 0.259 | 0.723 | 0.216 | 0.946 | 0.230 |
| $Fe^{3+}$ | 1.600 | 1.126 | 1.517 | 0.744 | 1.549 | 1.672 | 1.173 | 1.604 | 1.048 | 1.671 |
| $Fe^{2+}$ | 0.264 | 0.193 | 0.320 | 0.155 | 0.219 | 0.080 | 0.134 | 0.254 | 0.016 | 0.124 |
| Mn | 0.000 | 0.000 | 0.000 | 0.056 | 0.022 | 0.026 | 0.025 | 0.000 | 0.031 | 0.025 |
| Ca | 2.936 | 2.901 | 2.890 | 2.894 | 2.909 | 2.963 | 2.946 | 2.926 | 2.959 | 2.951 |
| End members | | | | | | | | | | |
| Pyrope | 0.0 | 0.0 | 0.0 | 0.0 | 0.0 | 0.0 | 0.0 | 0.0 | 0.0 | 0.0 |
| Almandine | 8.2 | 6.2 | 10.0 | 5.0 | 6.9 | 2.6 | 4.3 | 8.0 | 0.5 | 4.0 |
| Spessartine | 0.0 | 0.0 | 0.0 | 1.8 | 0.7 | 0.9 | 0.8 | 0.0 | 1.0 | 0.8 |
| Grossular | 2.9 | 34.7 | 5.3 | 53.9 | 8.6 | 10.0 | 33.0 | 3.9 | 45.9 | 7.3 |
| Andradite | 88.9 | 59.1 | 84.7 | 39.3 | 83.7 | 86.6 | 61.9 | 88.2 | 52.6 | 87.9 |
| Uvarovite | 0.0 | 0.0 | 0.0 | 0.0 | 0.0 | 0.0 | 0.0 | 0.0 | 0.0 | 0.0 |
| Total | 100.0 | 100.0 | 100.0 | 100.0 | 100.0 | 100.0 | 100.0 | 100.0 | 100.0 | 100.0 |

n.d. – not detected

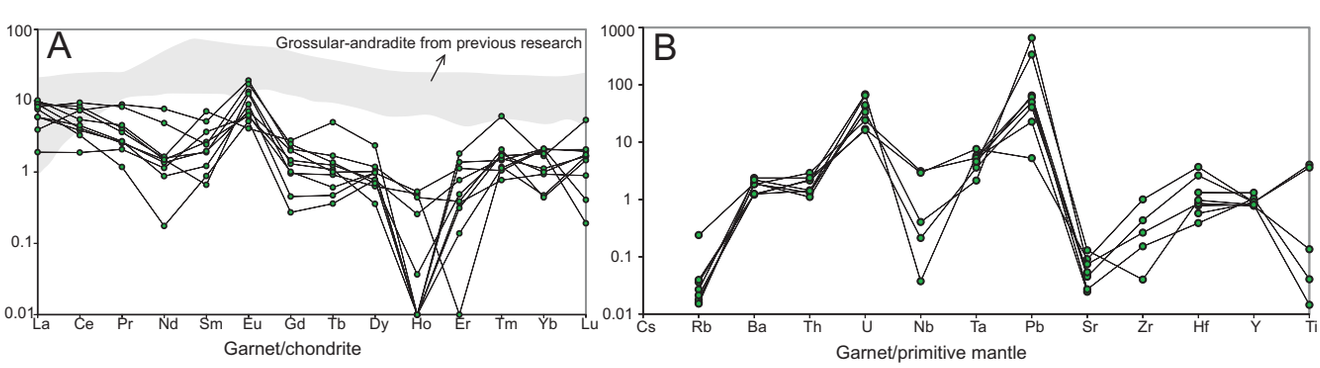


**Fig. 5A – chondrite-normalized REE pattern of Rudnik garnets; the shaded field is from previous research (Kostić et al., 2021); B – trace element spider diagram of the Rudnik garnets; the values obtained were normalized on basis of primitive mantle values (McDonough et al., 1995)**

Table 2

**Representative LA-ICP-MS trace element and REE data [ppm] on the Rudnik garnets**

| Spot no. | Cs | Rb | Ba | Th | U | Nb | Ta | Pb | Sr | Zr | Hf | Y | Ti |
|---|---|---|---|---|---|---|---|---|---|---|---|---|---|
| 1 | n.d. | 0.037 | 0.45 | 0.038 | 0.312 | n.d. | 0.061 | 0.161 | 0.363 | n.d. | 0.081 | 1.269 | n.d. |
| 2 | n.d. | 0.549 | 0.46 | 0.032 | 0.327 | n.d. | 0.073 | 0.056 | 0.178 | n.d. | 0.059 | 1.389 | n.d. |
| 3 | n.d. | 0.083 | 0.29 | 0.064 | 0.505 | 0.009 | 0.079 | 0.15 | 0.197 | 0.58 | 0.04 | 1.63 | 17.8 |
| 4 | n.d. | 0.035 | 1.6 | 0.071 | 0.157 | n.d. | 0.048 | 0.35 | 1.05 | 0.34 | 0.01 | 2.41 | 85 |
| 5 | n.d. | 0.041 | 0.44 | 0.084 | 0.179 | 0.75 | 0.072 | 0.123 | 0.326 | 1.65 | 0.27 | 1.405 | 1780 |
| 6 | n.d. | 0.091 | 0.3 | 0.062 | 0.125 | 0.7 | 0.103 | 0.013 | 0.66 | 3.82 | 0.38 | 1.415 | 1580 |
| 7 | n.d. | n.d. | n.d. | 0.097 | 0.114 | 0.249 | 0.04 | 2.32 | 0.55 | 1.59 | 0.159 | 2.61 | 592 |
| 8 | n.d. | 0.035 | 0.57 | 0.069 | 0.12 | 0.051 | 0.049 | 0.1 | 0.39 | n.d. | 0.136 | 2.06 | n.d. |
| 9 | n.d. | 0.062 | 0.53 | 0.042 | 0.249 | 0.097 | 0.029 | 1.62 | 0.54 | 1.01 | 0.088 | 1.217 | 59.5 |
| 10 | n.d. | 0.049 | 0.3 | 0.041 | 0.484 | n.d. | 0.062 | 0.83 | 0.94 | 0.153 | 0.1 | 1.272 | 6.4 |

n.d. – not detected

Tab. 2. cont.

| Spot no. | La | Ce | Pr | Nd | Sm | Eu | Gd | Tb | Dy | Ho | Er | Tm | Yb | Lu | REE | LREE/ HREE | Eu | Ce |
|---|---|---|---|---|---|---|---|---|---|---|---|---|---|---|---|---|---|---|
| 1 | 9.620 | 7.389 | 3.620 | 1.575 | 1.891 | 13.321 | 1.306 | 1.080 | 0.357 | 0.010 | 0.368 | 0.769 | 0.931 | 0.894 | 9.533 | 1.21 | 0.69 | 1.73 |
| 2 | 8.945 | 8.303 | 4.137 | 1.487 | 0.662 | 12.433 | 0.954 | 0.914 | 0.630 | 0.494 | 0.01 | 1.174 | 0.472 | 1.666 | 9.623 | 1.16 | 1.21 | 2.03 |
| 3 | 3.924 | 7.308 | 8.836 | 7.680 | 5.135 | 19.182 | 2.110 | 1.689 | 1.178 | 0.439 | 0.387 | 2.064 | 0.440 | 1.463 | 12.595 | 1.29 | 0.45 | 2.56 |
| 4 | 10.084 | 5.448 | 4.525 | 1.641 | 7.094 | 4.085 | 2.763 | 4.986 | 2.357 | 0.010 | 1.812 | 6.072 | 1.677 | 5.365 | 10.332 | 1.49 | 0.07 | 1.18 |
| 5 | 5.907 | 3.849 | 2.640 | 1.356 | 1.959 | 7.104 | 2.010 | 0.997 | 1.016 | 0.010 | 1.375 | 1.457 | 2.111 | 1.951 | 6.645 | 1.43 | 0.28 | 1.43 |
| 6 | 1.898 | 1.876 | 2.079 | 1.137 | 3.648 | 6.074 | 1.457 | 1.246 | 0.772 | 0.256 | 0.768 | 1.538 | 1.118 | 1.666 | 4.116 | 1.77 | 0.20 | 1.78 |
| 7 | 8.902 | 4.143 | 2.553 | 1.487 | 2.635 | 6.216 | 1.005 | 0.609 | 0.975 | 0.531 | 1.125 | 1.052 | 2.049 | 2.073 | 7.385 | 1.32 | 0.29 | 1.08 |
| 8 | 7.594 | 3.278 | 1.174 | 0.175 | 0.878 | 5.150 | 0.271 | 0.360 | 0.772 | 0.010 | 0.312 | 1.781 | 0.993 | 1.747 | 4.973 | 1.24 | 0.78 | 1.05 |
| 9 | 5.907 | 4.502 | 2.693 | 0.875 | 1.216 | 8.880 | 0.452 | 0.470 | 0.975 | 0.010 | 0.137 | 1.133 | 2.111 | 0.406 | 6.237 | 1.29 | 0.92 | 1.67 |
| 10 | 8.185 | 9.363 | 8.221 | 4.857 | 2.432 | 17.051 | 2.462 | 1.357 | 0.691 | 0.036 | 0.487 | 1.700 | 1.801 | 0.191 | 13.108 | 1.22 | 0.56 | 2.12 |

Table 3

**Representative data of fluid inclusion microthermometric measurements on the Rudnik garnets**

| Spot no. | Origin | Type | Size [μm] | Tm-ice [°C] | Th [°C] | Salinity wt.% NaCl equivalent | Density [g/cm$^3$] |
|---|---|---|---|---|---|---|---|
| 1 | P | L-V | 3.8 | –11.0 | 373 | 14.97 | 0.77 |
| 2 | P | L-V | 4.2 | –10.6 | 376 | 14.57 | 0.76 |
| 3 | P | L-V | 5.1 | –10.3 | 379 | 14.25 | 0.75 |
| 4 | P | L-V | 3.5 | –11.2 | 392 | 15.17 | 0.74 |
| 5 | P | L-V | 4.8 | –11.3 | 385 | 15.27 | 0.75 |

P – primary, L – liquid, V – vapour, Tm-ice – ice melting temperature, Th – total fluid homogenization temperature

ature (Th) from 373–392 C, while the salinity of the trapped fluid inclusion ranges from 14.25 to 15.27% NaCl equivalent. The estimated fluid inclusion densities are from 0.74 to 0.77 g/cm$^3$, calculated according to Bodnar (1993).

## DISCUSSION

The Rudnik garnets generally occur in proximal skarns close to the contact with igneous bodies such as sills and dykes

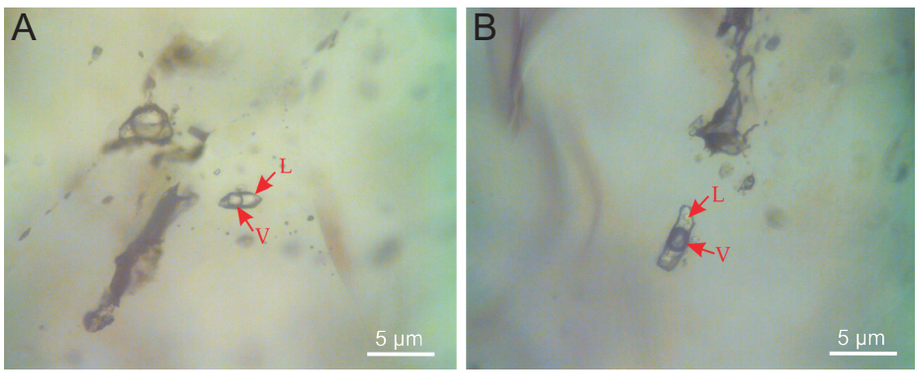


**Fig. 6A, B – images of liquid-vapour (L-V) type fluid inclusions trapped in the Rudnik garnets**

(Kostić et al., 2021). Garnets appear rarely in distal skarns, and they are closely controlled by hydrothermal fluid paths along sedimentary bed boundaries, and in local fractures and porosity zones (Kostić, 2021). One of the most important controlling factors for garnet in the Rudnik locality is the amount of carbonate component in the protolith (Kostić, 2021).

As the general garnet formula is $\{X\}_3[Y]_2(Z)_3O_{12}$, yttrium, U and REE incorporation in the garnet crystal structure is only possible by coupled substitution of $Ca^{2+}$ in the dodecahedral {X} position (Carlson et al., 2014). Generally, the Y/Ho ratio of garnet from hydrothermal systems is higher than the Y/Ho ratio from magmatic processes, where values are much closer to the chondrite value (Bau and Dulski, 1996). According to Gaspar et al. (2008), in hydrothermal systems Y can usually easily fractionate from Ho. Because Rudnik garnets have relatively high Y/Ho ratios, i.e., ranging from 51.4 to 636 (average 133), this suggests that processes responsible for their crystallization originate from hydrothermal activity.

Therefore, the incorporation of REEs and trace elements into garnet crystals can be controlled by fluid-rock interaction (Liang et al., 2021), because the Y, U and $REE^{3+}$ in the Rudnik garnets do not display an apparent linear relationship. Namely, the total Al and $Fe^{3+}$ contents are not correlated with the $REE^{3+}$ contents, suggesting that the substitution mechanism is not of the YAG-type (Fig. 7).

It is well-known that garnets which exhibit LREE depletion with a negative or absent Eu anomaly originate from neutral hydrothermal fluids (Bau, 1991). The relaxation energy for $Eu^{2+}$ which replaces Ca, i.e., which enters into the dodecahedral {X} site in garnet, is lower than needed for the trivalent Eu. Also, in hydrothermal systems, the presence of $Cl^-$ under mildly acidic conditions can significantly control REE patterns and amplify the stability of soluble $Eu^{2+}$. Acidic conditions favour $Eu^{2+}$ transportation in hydrothermal fluids and form positive Eu anomalies (Gaspar et al., 2008). In a previous study (Kostić et al., 2021), it was demonstrated that grossularite-rich garnets from the proximal zone close to contact with the igneous body:

- have LREE-depleted patterns;
- have HREE-enriched patterns;
- have no positive or negative Eu anomaly (Fig. 5A);
- were formed by prolonged interaction of pore fluids with the host rock.

Gaspar et al. (2008) suggested that a distinct positive Eu anomaly occurs under acidic conditions.

By contrast, the garnets studied here from the Rudnik distal skarn zone are more andradite-rich, and they display:

- LREE-enriched patterns;
- HREE-depleted patterns;
- a positive Eu anomaly;
- they originate from magma-derived hydrothermal fluids of acidic nature.

In fluid systems, a reduction in U solubility may be caused by a decrease in $fO_2$, and this process increases U incorporation into garnet (Zhang et al., 2017). In the Rudnik garnets, U concentrations are the range 0.114 to 0.505 ppm (Table 2), and the average value is 0.257 ppm, whereas lower U concentrations reveal that garnets have crystallized under increased oxygen fugacity conditions.

As garnets are stable at higher temperatures, trapped fluid inclusions in the garnet can be considered as primary inclu-

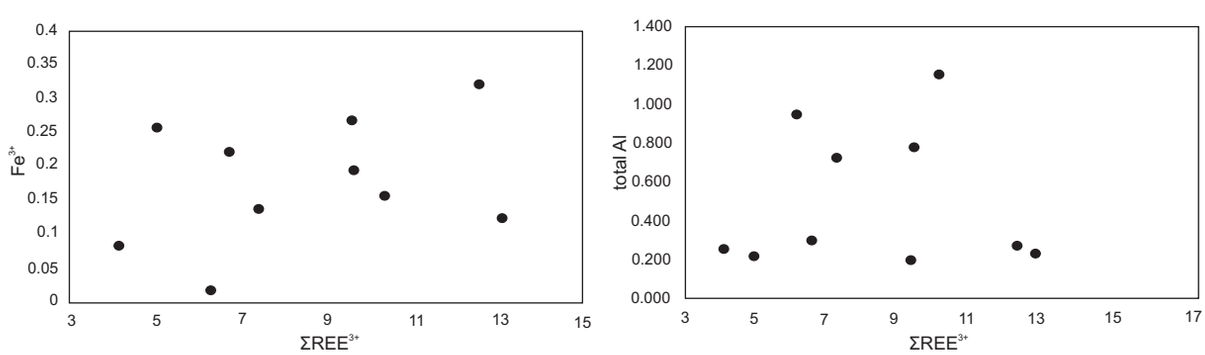


**Fig. 7. Diagrams of total Al and $Fe^{3+}$ contents *versus* $REE^{3+}$ contents**

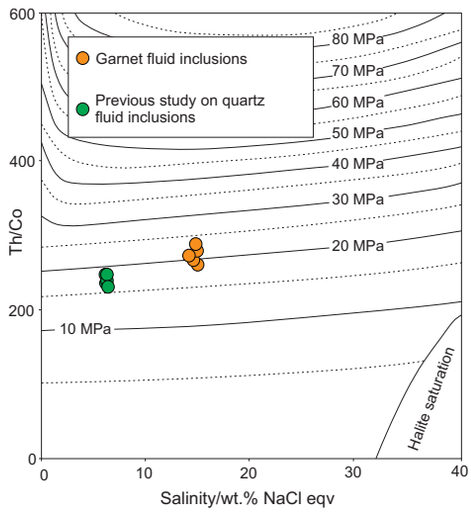


**Fig. 8. Homogenization temperature *versus* salinity plots of fluid inclusion assemblages**

Data for quartz fluid inclusions (green fields) are from a previous study (Kostić, 2021)

sions, as they relate to the garnet growing zones. Homogenization temperature (Th) data were used to calculate the PT conditions of fluids at the moment of garnet crystallization. To reveal the minimum trapping pressure of the primary inclusions in the Rudnik garnets, the results obtained are plotted on a diagram of Driesner and Heinrich (2007). Homogenization temperatures *versus* salinity plotted on the diagram in Figure 8 show that the trapping pressure is between 19 and 23 MPa. Compared with data from fluid inclusions in quartz described in Kostić (2021), fluid inclusions in the garnet have somewhat higher fluid trapping pressures.

In previous research (Kostić et al., 2021), Al-rich garnets from the proximal exoskarn have a flat to moderate upward-sloping (LREE-depleted and HREE-enriched) trend with little or no Eu anomaly (Fig. 5A). Garnets from distal exoskarns have obvious LREE-enriched and flat HREE patterns with a strong positive Eu anomaly. The positive Eu anomalies in the exoskarn garnets indicate that Eu mainly occurred as $Eu^{2+}$ in the fluids, and the composition of the hydrothermal fluids evolved from the proximal to distal skarns.

Sverjensky (1984) experimentally showed that in skarn systems divalent Eu should predominate >250°C. Results from fluid inclusion microthermometry (Table 3) on the Rudnik garnets indicate that homogenization temperatures of the fluid inclusions are above 250°C and indicate that the Rudnik garnets formed at higher temperatures (about homogenization temperature or more).

Furthermore, previous research (Cvetković et al., 2016; Kostić et al., 2021) followed an earlier hypothesis concerning the links between the origin of the Rudnik mineralization, garnet crystallization, and magmatic-hydrothermal activity. Particularly, the Rudnik garnet primarily originated from infiltration metasomatism induced by hydrothermal fluids along the contact zone between dykes and sedimentary layers, fractures and porosity zones.

## CONCLUSIONS

The major findings of this study can be summarized as follows:

1. Garnets are rare in the distal skarns of Rudnik, and their presence is strongly linked to the paths of hydrothermal fluids through the contact zones between sedimentary layers, fractures, and porous zones.
2. A high Y/Ho ratio suggests that processes responsible for garnet crystallization originate from activity related to hydrothermal fluids.
3. In comparation to the proximal skarns, garnets found in the distal skarns of Rudnik are characterized by higher Fe contents, positive Eu anomalies, and an enrichment in light rare earth elements (LREE) with a flat pattern for heavy rare earth elements (HREE).
4. The low U concentrations observed in garnets indicate that they crystalized under conditions of increased oxygen fugacity.
5. The garnets were formed from hydrothermal fluids under physicochemical conditions characterized by minimum temperatures of 373–392°C, minimum trapping pressures of 19–23 MPa, mildly acidic pH levels, and increased oxygen fugacity.

**Acknowledgements**. This paper has been financed by the „Contract on realization and financing of scientific research of SRI in 2024“, Nr. 451-03-65/2024-03/ 200126. The authors thank the Laboratory for Fluid Inclusions, Faculty of Mining and Geology, University of Belgrade, for support, and to anonymous referees for helpful comments and criticisms.

## REFERENCES

**Anđelković, M., 1973.** Geology of Mesozoic vicinity of Belgrade (in Serbian). Annales Geologiques de la Peninsule Balkanique, **38**: 1–136.

**Bau, M., 1991.** Rare-earth element mobility during hydrothermal and metamorphic fluid-rock interaction and the significance of the oxidation state of europium. Chemical Geology, **93**: 219–230. https://doi.org/10.1016/0009-2541(91)90115-8

**Bau, M., Dulski, P., 1996.** Anthropogenic origin of positive gadolinium anomalies in river waters. Earth and Planetary Science Letters, **143**: 245–255. https://doi.org/ 10.1016/0012-821X(96)00127-6

**Brković, T., 1980.** Explanatory booklet for sheet Kragujevac (in Serbian with English summary). In: Basic Geological Map of Yugoslavia 1:100,000. Federal Geological Institute, Belgrade.

**Brković, T., Radovanović, Z., Pavlović, Z., Dimitrijević, M., 1980.** Geological Map of Yugoslavia 1:100 000, sheet Kragujevac. Federal Geological Institute, Belgrade.

**Bodnar, R., 1993.** Revised equation and table for determining the freezing point depression of $H_2O$-NaCl solutions. Geochimica et Cosmochimica Acta, **57**: 683–684. https://doi.org/10.1016/0016-7037(93)90378-A

**Carlson, W., Gale, J., Wright, K., 2014.** Incorporation of Y and REEs in aluminosilicate garnet: energetics from atomistic simulation. American Mineralogist, **99**: 1022–1034. https://doi.org/10.2138/am.2014.4720

**Ciobanu, L.C., Cook, I.N., 2004.** Skarn textures and a case study: the Ocna de Fier-Dognecea orefield, Banat, Romania. Ore Geology Reviews, **24**: 315–370. https://doi.org/10.1016/j.oregeorev.2003.04.002

**Cvetković, V., Šarić, K., Pécskay, Z., Gerdes, A., 2016.** The Rudnik Mts. volcano-intrusive complex (central Serbia): an example of how magmatism controls metallogeny. Geologia Croatica, **69**: 89–99. https://doi.org/10.4154/GC.2016.08

**Dimitrijević, M.N., Dimitrijević, M.D., 1987.** The Turbiditic Basins of Serbia. Serbian Academy of Sciences and Arts Department of Natural and Mathematical Sciences, Belgrade.

**Dimitrijević, M.N., Dimitrijević, M.D., 2009.** The Lower Cretaceous paraflysch of the Vardar zone: composition and fabric. Annales Geologiques de la Peninsule Balkanique, **70**: 9–21.

**Driesner, T., Heinrich, A., 2007.** The system $H_2O$-NaCl. Part I: correlation formulae for phase relations in temperature-pressure-composition space from 0 to 1000°C, 0 to 5000 bar, and 0 to 1 $X_{NaCl}$. Geochimica et Cosmochimica Acta, **71**: 4880–4901. https://doi.org/10.1016/j.gca.2006.01.033

**Einaudi, M.T., Meinert, L.D., Newbery, R.J., 1981.** Skarn deposits. Economic geology, 75th Anniversary Volume: 317–391. https://doi.org/10.2113/gsecongeo.95.6.1183

**Filipović, I., Pavlović, Z., Marković, B., Rodin, V., Marković, O., Gagić, N., Atin, B., Milićević, M., 1978.** Geological Map of Yugoslavia 1:100 000, sheet Gornji Milanovac. Federal Geological Institute, Belgrade.

**Gaspar, M., Knaack, C., Meinert, D.L., Moretti, R., 2008.** REE in skarn systems: A LA-ICP-MS study of garnets from the Crown Jewel gold deposit. Geochimica et Cosmochimica Acta, **72**: 185–205. https://doi.org/10.1016/j.gca.2007.09.033

**Haas, J., Péró, C., 2004**. Mesozoic evolution of the Tisza Megaunit. International Journal of Earth Sciences, **93**: 297–313. http://doi.org/10.1007/s00531-004-0384-9

**Jamtveit, B., Hervig, R.L., 1994.** Constraints on transport and kinetics in hydrothermal systems from zoned garnet crystals. Science, **263**: 505–508. https://doi.org/10.1126/science.263.5146.505

**Jamtveit, B., Wogelius, R., Fraser, D., 1993.** Zonation patterns of skarn garnets: records of hydrothermal system evolution. Geology, **21**: 113–116. https://doi.org/10.1130/0091-7613(1993)021<0113:ZPOSGR>2.3.CO;2

**Jamtveit, B., Ragnarsdottir, K.V., Wood, B.J., 1995.** On the origin of zoned grossular-andradite garnets in hydrothermal systems. European Journal of Mineralogy, **7**: 1399–1410. https://doi.org/10.1127/ejm/7/6/1399

**Kostić, B., 2021.** Contact metamorphism of Upper Cretaceous sedimentary rocks of Rudnik. Ph.D. Thesis, University of Belgrade, Faculty of Mining and Geology.

**Kostić, B., Srećković-Batoćanin, D., Filipov, P., Tančić, P., Sokol, K., 2021**. Anisotropic grossular-andradite garnets: evidence of two stage skarn evolution from Rudnik, Central Serbia. Geologica Carpathica, **72**: 17–25. https://doi.org/10.31577/GeolCarp.72.1.2

**Liang, P., Zhang, Y., Xie, Y., 2021**. Chemical composition and genesis implication of garnet from the Laoshankou Fe-Cu-Au deposit, the northern margin of East Junggar, NW China. Minerals, **11**: 334. https://doi.org/10.3390/min11030334

**McDonough, W.F., Sun, S., 1995.** The composition of the Earth. Chemical Geology, **120**: 223–253. https://doi.org/10.1016/0009-2541(94)00140-4

**Nicolescu, S., Cornell, D., Sodervall, U., Odelius, H., 1998.** Secondary ion mass spectrometry analysis of rare earth elements in grandite garnet and other skarn related silicates. European Journal of Mineralogy, **10**: 251–259. https://doi.org/10.1127/ejm/10/2/0251

**Pamić, J., Šparica, M., 1983.** The age of the volcanic of Požeška Gora (Croatia, Yugoslavia). Radovi Jugoslovenske Akademije Znanosti i Umjetnosti, **404**: 183–198.

**Park, C., Song, Y., Kang, I., Shim, J., Chung, D., Park, C., 2017.** Metasomatic changes during periodic fluid flux recorded in grandite garnet from the Weondong W-skarn deposit, South Korea. Chemical Geology, **451**: 135–153. https://doi.org/10.1016/j.chemgeo.2017.01.011

**Paton, C., Hellstrom, J., Paul, B., Woodhead, J., Hergt, J., 2011.** Iolite: freeware for the visualization and processing of mass spectrometric data. Journal of Analytical Atomic Spectrometry, **26**: 2508–2512. https://doi.org/10.1039/c1ja10172b

**Pollok, K., Jamtveit, B., Putnis, A., 2001.** Analytical transmission electron microscopy of osscillatory zoned grandite garnets. Contributions to Mineralogy and Petrology, **141**: 358–366. https://doi.org/10.1007/s004100100248

**Prelević, D., Wehrheim, S., Reutter, M., Romer, R., Boev, B., Božović, M., Bogaard, P., Cvetković, V., Schmid, S., 2017**. The Late Cretaceous Klepa basalts in Macedonia (FYROM) – Constrains on the final stage of Tethys closure in the Balkans. Terra Nova, **23**: 145–153. https://doi.org/10.1111/ter.12264

**Schmid, M., Bernoulli, D., Fügenschuh, B., Matenco, L., Schefer, S., Schuster, R., Tischler, M., Ustaszewski, K., 2008**. The Alpine-Carpathian-Dinaridic orogenic system: correlation and evolution of tectonic units. Swiss Journal of Geoscience, **101**: 139–183. https://doi.org/10.1007/s00015-008-1247-3

**Sladić-Trifunović, M., Pantić, N., Mihajlović, Đ., 1989.** The significance of clastic limestone in the section of Bela Reka-Resnik, for stratigraphic interpretation and reconstruction of the depositional environments of the Upper Jurassic-Lower Cretaceous deep-complexes in the vicinity of Belgrade. In: Proceedings *SGD* for 1987, 1988 and 1989.

**Smith, M., Henderson, P., Jeffries, T., Long, J., Williams, C., 2004.** The rare earth elements and uranium in garnets from the Beinn an Dubhaich aureole, Skye, Scotland, UK: constraints on processes in a dynamic hydrothermal system. Journal of Petrology, **45**: 457–484. https://doi.org/10.1093/petrology/egg087

**Somarin, A.K., 2004**. Garnet composition as an indicator of Cu mineralization: evidence from skarn deposit of NW Iran. Journal of Geochemical Exploration, **81**: 47–57. https://doi.org/10.1016/S0375-6742(03)00212-7

**Srećković-Batoćanin, D., Vasković, N., Milutinović, S., Ilić, V., Nikić, Z., 2014.** Composition of zonal garnets from the garnetite exoskarn of the ore field Rogozna (Rogozna Mts, southern Serbia). Proceedings of the XVI Serbian Geological Congress. Donji Milanovac: 265–269.

**Stojanović, J., Radosavljević, S., Tošović, R., Pačevski, A., Radosavljević-Mihaljović, A., Kašić, V., Vuković, N., 2018.** A review of the Pb-Zn-Cu-Ag-Bi-W polymetallic ore from the Rudnik orefield, Central Serbia. Annales Geologiques de la Peninsule Balkanique, **79**: 47–69.

**Sverjensky, D.A., 1984.** Europium redox equilibria in aqueous solution. Earth and Planetary Science Letters, **67**: 70–78. https://doi.org/10.1016/0012-821X(84)90039-6

**Tančić, P., Vulić, P., Kaindl, R., Sartory, B., Dimitrijević, R., 2012.** Macroscopically-zoned grandite from the garnetite skarn of Meka Presedla (Kopaonik Mountain, Serbia). Acta Geologica Sinica, **86**: 393–406. https://doi.org/10.1111/j.1755-6724.2012.00668.x

**Tančić, P., Kremenović, A., Vulić, P., 2020**. Structural dissymmetrization of optically anisotropic $Grs_{64\ \pm1}Adr_{36\ \pm1}Sps_2$ grandite from Meka Presedla (Kopaonik Mt., Serbia). Powder Diffraction, **35**: 7–16. https://doi.org/10.1017/S0885715619000897

**Whitney, D., Evans, B., 2010**. Abbreviations for names of rock-forming minerals. American Mineralogist, **95**: 185–187. https://doi.org/10.2138/am.2010.3371

**Xiao, X., Zhou, T., White, N., Zhang, L., Fan, Y., Wang, F., Chen, X., 2018**. The formation and trace elements of garnet in the skarn zone from the Xinqiao Cu-S-Fe-Au deposit, Tongling ore district, Anhui Province, Eastern China. Lithos, **302–303**: 467–479. https://doi.org/10.1016/j.lithos.2018.01.023

**Yardley, D.W.B., Rochelle, A.C., Barnicoat, C.A., Lloyd, E.G., 1991**. Oscillatory zoning in metamorphic minerals: an indicator of infiltration metasomatism. Mineralogical Magazine, **55**: 357–365. https://doi.org/10.1180/MINMAG.1991.055.380.06

**Zhai, D., Liu, J., Zhang, H., Wang, J., Su, L., Yang, X., Wu, S., 2014**. Origin of oscillatory zoned garnets from the Xieertala Fe-Zn skarn deposit, northern China: in situ LA-ICP-MS evidence. Lithos, **190–191**: 279–291. https://doi.org/10.1016/j.lithos.2013.12.017

**Zhang, Y., Qingquan, L., Yongjun, S., Hongbin, L., 2017**. Fingerprinting the hydrothermal fluid characteristics from LA-ICP-MS trace element geochemistry of garnet in the Yongping Cu deposit, SE China. Minerals, **7**: 199. https://doi.org/10.3390/min7100199